Research Report

2014-39

Dynamics and Vector Control of Wound-Rotor Brushless Doubly Fed Induction Machines

Z. S. Du, T. A. Lipo

Dept. of Elect. & Comp. Engr.
University of Wisconsin-Madison
1415 Engineering Drive
Madison, WI 53706

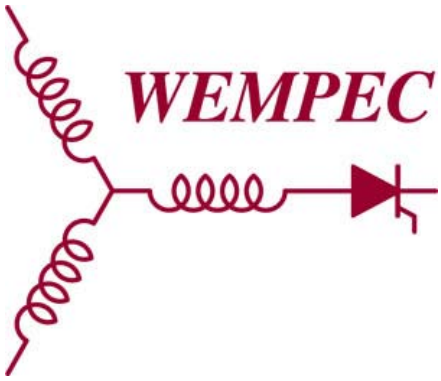

Wisconsin
Electric
Machines &
Power
Electronics
Consortium

University of Wisconsin-Madison
College of Engineering
Wisconsin Power Electronics Research Center
2559D Engineering Hall
1415 Engineering Drive
Madison WI 53706-1691

Dynamics and Vector Control of Wound-Rotor Brushless Doubly Fed Induction Machines

Zhentao S. Du
Dept. of Electrical and Computer Engineering
University of Wisconsin-Madison
Madison, WI 53706 USA
Email: zdu4@wisc.edu

Thomas A. Lipo
Dept. of Electrical and Computer Engineering
University of Wisconsin-Madison
Madison, WI 53706 USA
Email: lipo@engr.wisc.edu

***Abstract*—This paper proposes a Wound-Rotor Brushless Doubly Fed Induction Machine (WRBDFIM), an alternative Brushless Doubly Fed Induction Machine (BDFIM) concept for wind turbine applications. The WRBDFIM consists of two separate machine winding sets different in pole-numbers, whose rotor windings are connected together. Both of the winding sets are housed in the same machine frame. The separate winding set arrangement aims to eliminate the circulating current and suppress the undesired spatial harmonics created by the conventional BDFIM. The two-phase equivalent circuit of the WRBDFIM is derived by connecting the circuits of two conventional Doubly Fed Induction Machines (DFIMs). The electrical and mechanical dynamics are identified to form the machine model for the Direct Power Vector Control (DPVC), which is proposed to regulate the generated power of the WRBDFIM without rotor position sensors. Simulation results confirm the machine dynamic model and also prove the effectiveness of the DPVC scheme that provides accurate control and fast tracking capability.**

I. Introduction

Wind power generation, a key renewable energy technology, converts natural wind power to electrical power in a clean, efficient, and cost-effective manner through the usage of a wind turbine and an electrical generator. The Doubly Fed Induction Generator (DFIG) is one of the current main players in wind power generation due to their lower size drive requirement (approximately 30% of the rated power [1]) comparing to that of other machines; and the slip power recovery, which serves to further improve efficiency. [2] The main drawback of DFIGs is the presence of the brushes and slip rings used to enable access to the rotor terminals. Due to the direct contact between the rotor and the brushes, the brushes are worn out within a regular period of time. Besides the construction cost, the maintenance cost significantly increases the overall cost of a wind-turbine unit from a long term perspective.

The design of conventional Brushless Doubly Fed Induction Machines (BDFIMs) is based on the cascaded induction machine principle devised by Hunt [3], which uses a single set of stator windings to produce two spatial Magnetomotive Forces (MMFs), different in pole-numbers, rotating in the air gap, which interact with a nested-loop rotor. [4]–[8] While this design eliminates the costly usage of brushes and slip rings, the main drawbacks of the conventional BDFIMs design are the choice of the single stator winding set and the complex design of the nested-loop rotor. The single stator winding set creates an unbalanced mutual inductance, resulting in a circulating current flowing through the phase windings, which leads to higher copper loss. [9] The nested-loop rotor has been proven to create other unwanted spatial harmonics [10] that impair the performance of the machine.

Brushless Doubly Fed Reluctance Machines (BDFRMs), the counterparts of BDFIMs, are claimed to offer higher efficiency since their salient rotors do not require copper conductors. [11]–[13] In addition, BDFRMs could potentially ease the rotor manufacture. Thus far, a quantitative comparison of features between the BDFIM and BDFRM has no yet appeared. However, in the case of normal singly fed machines, use of reluctance machines is rare and induction machines have retained their favor over reluctance machines because of their better power factor/efficency product and overload capability among others. It is not unseemly to expect these same advantages may also pertain to doubly fed configurations as well. In any case the issue of the pros and cons of these two solutions are an interesting subject of future research but not the issue of this paper.

This paper proposes a different type of BDFIM, namely the Wound-Rotor Brushless Doubly Fed Induction Machine (WRBDFIM), which is essentially a connection of two Doubly Fed Induction Machines (DFIMs) with different pole-pair number housed in the same frame. The fundamental mutual inductance between the two winding sets is zero and the higher harmonic mutual inductances are so small that they are neglected in this paper. In fact, the existence of these harmonic mutual couplings creates small amount of undesired torque ripple; however the torque ripple is significantly reduced compared to that of conventional BDFIMs using a nested-loop rotor due to the choice of the separate rotor winding sets in the WRBDFIM. Furthermore, the stator of the WRBDFIM has two separate stator winding sets purposely to eliminate the circulating current [9] in the stator windings of conventional BDFIMs where the two stator currents share the common stator winding set to create two distinctive pole-pair magnetic fields.

The configuration of the WRBDFIM is shown in Fig. 1. The stator winding set that connects directly to the grid is called the Main Machine Winding Set (MMWS); the other

978-1-4799-5776-7/14/$31.00

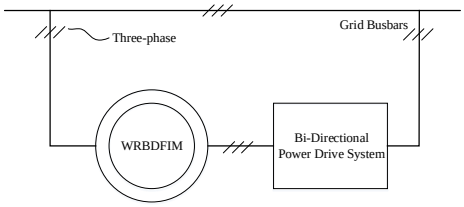

Fig. 1. The configuration of the WRBDFIM with an AC drive.

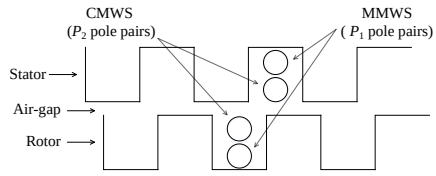

Fig. 2. The stator and rotor winding scheme of the WRBDFIM. Note: P_1 and P_2 are the number of pole pairs of the MMWS and CMWS respectively. Henceforth, '1' and '2' denote a MMWS and CMWS quantity, respectively.

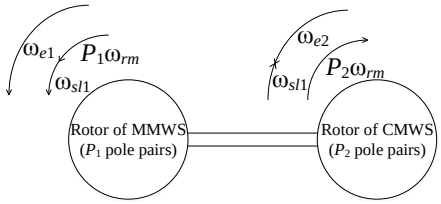

Fig. 3. The speed vector diagram summarizes all the flux waves rotating in the air-gap. Note: ω_{e1}, ω_{rm}, ω_{sl1}, ω_{e2} denote the main machine grid-excitation frequency, the rotor mechanical frequency, the main machine slip frequency, and the control machine induction frequency, respectively.

stator winding set that connects to the inverter is called the Control Machine Winding Set (CMWS). The MMWS and the CMWS are shorted with each other on the rotor. At the point of connection between the two rotor windings, the A-phase, B-phase, and C-phase of the MMWS are connected to the A-phase, C-phase, and B-phase of the CMWS, respectively. The purpose of the reverse phase sequence is mainly to reverse the direction of the rotating MMF of the rotor of the CMWS.

The structure of the machine is the same as that of the conventional wound-rotor induction machine with two-layer windings. The slots accommodate the two sets of windings in both the stator and rotor, as shown in Fig. 2. The machine is easier to manufacture compared to that of the counterpart BDFRM. The two-phase equivalent circuit of the WRBDFIM is readily derived, followed by the modelling of the machine dynamics. In addition, this paper proposes a new vector control design for the proposed WRBDFIMs based on the work [14] for DFIMs, which features an accurate, robust, and feasible DPVC scheme without rotor position sensors that are essential in the control schemes proposed by [8], [15], [16].

II. Operating Principle

The WRBDFIM produces average torque only if the frequency of the excitation applied to the stator terminals of the CMWS is in synchronization with the frequency that is induced in the stator CMWS. Such a rotating frequency can be obtained using a speed vector diagram, as shown in Fig. 3, which summarizes all the frequencies of the flux waves rotating in the air gap. Let the rotor be rotating at the mechanical angular frequency ω_{rm}, the frequency of the flux wave induced due to the rotor MMWS is equal to the main machine slip frequency, as shown in (1).

$$\omega_{sl} = \omega_{e1} - P_1\omega_{rm} \tag{1}$$

Since the phase sequence is reversed at the point of rotor connection, the flux wave due to the rotor CMWS is opposite to the main machine slip frequency, i.e. $-\omega_{sl1}$. Since the rotor itself is rotating at ω_{rm}, the resultant speed vector in reference to the stator frame of the CMWS is equal to the frequency induced in the stator CMWS, i.e.

$$\omega_{e2} = -\omega_{sl1} + P_2\omega_{rm} \tag{2}$$

It should be noted that both rotor winding sets share the same mechanical rotor frequency; however, their electrical rotor frequencies are different due to their difference in pole numbers. The slip of each machine can be identified based on the definition in [5]. The cascaded-slip is the product of two individual slips, i.e.

$$\begin{aligned} s_{12} = s_1 s_2 &= \frac{\omega_{e1} - P_1\omega_{rm}}{\omega_{e1}} \cdot \frac{-\omega_{sl1} + P_2\omega_{rm}}{\omega_{e1} - P_1\omega_{rm}} \\ &= \frac{\omega_{e1} - (P_1 + P_2)\omega_{rm}}{\omega_{e1}} \end{aligned} \tag{3}$$

The cascaded slip in (3) reveals that the resultant pole pairs of the WRBDFIM are the sum of the pole-pairs of each winding set.

III. Two-phase Equivalent Circuit

For the purpose of modeling and control, the connection between the two DFIM winding sets made in the three phase domain is required to transform to the two-phase domain. The two-phase equivalent circuit for each DFIM is exactly the same as that of a conventional DFIM. The additional circuit connecting the two two-phase DFIM equivalent circuits is the junction circuit at the point of connection of the two rotor winding sets. Due to the changed phase sequence in the CMWS, the two-phase rotor voltage and current of the CMWS are different from those of the MMWS, although the two winding sets are both physically connected in the three-phase domain. The two-phase rotor voltage and current of the CMWS in its rotor frame can be expressed in terms of the corresponding rotor voltage and current of the MMWS in its rotor frame, with the zero-sequence set to zero, as in (4-5).

$$\begin{bmatrix} i^{r2}_{qr2} \\ i^{r2}_{dr2} \\ 0 \end{bmatrix} = -\mathbf{TS}\left(\mathbf{T}^{-1}\begin{bmatrix} i^{r1}_{qr1} \\ i^{r1}_{dr1} \\ 0 \end{bmatrix}\right) = -\begin{bmatrix} i^{r1}_{qr1} \\ -i^{r1}_{dr1} \\ 0 \end{bmatrix} \tag{4}$$

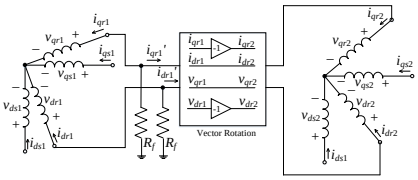

Fig. 4. The two-phase equivalent circuit of the WRBDFIM.

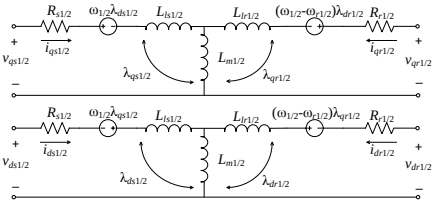

Fig. 5. The two-phase equivalent circuit of each individual winding set.

$$\begin{bmatrix} v_{qr2}^{r2} \\ v_{dr2}^{r2} \\ 0 \end{bmatrix} = \mathbf{TS} \left(\mathbf{T}^{-1} \begin{bmatrix} v_{qr1}^{r1} \\ v_{dr1}^{r1} \\ 0 \end{bmatrix} \right) = \begin{bmatrix} v_{qr1}^{r1} \\ -v_{dr1}^{r1} \\ 0 \end{bmatrix} \tag{5}$$

where

$$\mathbf{T} = \begin{bmatrix} 2/3 & -1/3 & -1/3 \\ 0 & -\sqrt{3}/3 & \sqrt{3}/3 \\ 1/3 & 1/3 & 1/3 \end{bmatrix} \tag{6}$$

and

$$\mathbf{S} = \begin{bmatrix} 1 & 0 & 0 \\ 0 & 0 & 1 \\ 0 & 1 & 0 \end{bmatrix} \tag{7}$$

In (4-5), $\mathbf{T}$ is the two-phase transformation matrix and $\mathbf{S}$ is the matrix that swaps the B- and C-phase elements of the three-phase voltage or current vector, and the superscripts indicate the frame of reference. The '$-$' sign in (4) is due to the change of current convention when transferring from one machine to another.

Based on the relationships listed in (4-5), the change of sequence at the point of the two rotor winding connection is equivalent to a vector rotation which rotates the *d*-phase elements of the rotor CMWS to be 180° away from those of the MMWS. After adding this vector rotation block at the junction of the two DFIMs, the overall two-phase equivalent circuit of the WRBDFIM can be drawn, as in Fig. 4. This two-phase equivalent circuit model restricts the voltages and currents of both winding sets to be referenced to their corresponding rotor frame. It should be noted that (4-5) are still valid in their corresponding synchronous frame where the voltages and currents are DC quantities. The vector rotation cannot be applied in any other frames as (4-5) are no longer valid.

IV. Dynamics of The WRBDFIM

The electrical dynamics of the WRBDFIM can be obtained based on the two-phase equivalent circuit depicted in Fig. 4. Based on the two-phase equivalent circuit of each DFIM shown in Fig. 5, the voltage equations of the *dq* phases are

$$v_{qs1/2} = r_{s1/2} i_{qs1/2} + p\lambda_{qs1/2} + \omega_{1/2}\lambda_{ds1/2} \tag{8}$$

$$v_{ds1/2} = r_{s1/2} i_{ds1/2} + p\lambda_{ds1/2} - \omega_{1/2}\lambda_{qs1/2} \tag{9}$$

$$v_{qr1/2} = r_{r1/2} i_{qr1/2} + p\lambda_{qr1/2} + (\omega_{1/2} - \omega_{r1/2})\lambda_{dr1/2} \tag{10}$$

$$v_{dr1/2} = r_{r1/2} i_{dr1/2} + p\lambda_{dr1/2} - (\omega_{1/2} - \omega_{r1/2})\lambda_{qr1/2} \tag{11}$$

where p is the differential operator, ω is the angular frequency of the reference frame, all the rotor quantities are stator-referred, and the subscript '1' or '2' stands for the MMWS quantity or the CMWS quantity, respectively. The voltage equations are generally rearranged to a state-space form that is commonly used in machine simulation. By rearranging (8-11) and using the flux to replace all the current terms, the electrical dynamics of the WRBDFIM are expressed in (12-15) in terms of flux states,

$$\begin{aligned} \dot{\lambda}_{qs1/2} = &\left(\frac{r_{s1/2} L_{m1/2}^*}{L_{ls1/2}^2} - \frac{r_{s1/2}}{L_{ls1/2}} \right) \lambda_{qs1/2} \\ &+ \frac{r_{s1/2} L_{m1/2}^* \lambda_{qr1/2}}{L_{ls1/2} L_{lr1/2}} \\ &- \omega_{1/2}\lambda_{ds1/2} + v_{qs1/2} \end{aligned} \tag{12}$$

$$\begin{aligned} \dot{\lambda}_{ds1/2} = &\left(\frac{r_{s1/2} L_{m1/2}^*}{L_{ls1/2}^2} - \frac{r_{s1/2}}{L_{ls1/2}} \right) \lambda_{ds1/2} \\ &+ \frac{r_{s1/2} L_{m1/2}^* \lambda_{dr1/2}}{L_{ls1/2} L_{lr1/2}} \\ &+ \omega_{1/2}\lambda_{qs1/2} + v_{ds1/2} \end{aligned} \tag{13}$$

$$\begin{aligned} \dot{\lambda}_{qr1/2} = &\left(\frac{r_{r1/2} L_{m1/2}^*}{L_{lr1/2}^2} - \frac{r_{r1/2}}{L_{lr1/2}} \right) \lambda_{qr1/2} \\ &+ \frac{r_{r1/2} L_{m1/2}^* \lambda_{qs1/2}}{L_{ls1/2} L_{lr1/2}} \\ &- (\omega_{1/2} - \omega_{r1/2})\lambda_{dr1/2} + v_{qr1/2} \end{aligned} \tag{14}$$

$$\begin{aligned} \dot{\lambda}_{dr1/2} = &\left(\frac{r_{r1/2} L_{m1/2}^*}{L_{lr1/2}^2} - \frac{r_{r1/2}}{L_{lr1/2}} \right) \lambda_{dr1/2} \\ &+ \frac{r_{r1/2} L_{m1/2}^* \lambda_{ds1/2}}{L_{ls1/2} L_{lr1/2}} \\ &+ (\omega_{1/2} - \omega_{r1/2})\lambda_{qr1/2} + v_{dr1/2} \end{aligned} \tag{15}$$

where

$$L_{m1/2}^* = L_{m1/2} // L_{ls1/2} // L_{lr1/2} \tag{16}$$

The voltage terms in (12-15) form the forcing vector of the WRBDFIM. The stator voltages of the MMWS and the CMWS are supplied by external sources. To identify the rotor voltage at the junction, a set of fictitious shunt resistors R_f are added as shown in Fig. 4. The resistance is set to a large value, forcing the current on both sides of each shunt resistor to be the same. The additional voltage equations at the junction can be drawn in (17-18) by using (4),

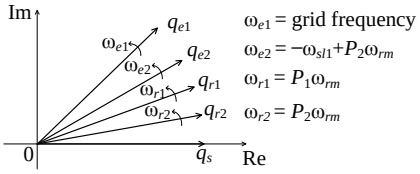

Fig. 6. Frames of reference of the MMWS and the CMWS. Note: subscripts 's', '$r1$', '$r2$', '$e1$', and '$e2$' denote the common stator frame, the rotor frame of the MMWS, the rotor frame of the CMWS, the synchronous frame of the MMWS, and the synchronous frame of the CMWS, respectively; the angular frequency of the synchronous frame of the CMWS must comply with the frequency criterion given in (2).

$$v_{qr1}^{r1} = -(i_{qr1}^{r1} + i_{qr1}^{r1\,\prime})R_f = -(i_{qr1}^{r1} + i_{qr2}^{r2})R_f \tag{17}$$

$$v_{dr1}^{r1} = -(i_{dr1}^{r1} + i_{dr1}^{r1\,\prime})R_f = -(i_{dr1}^{r1} - i_{dr2}^{r2})R_f \tag{18}$$

where the currents of (17-18) are related to the flux states in (12-15). In addition, the rotor voltage of the CMWS can be found using (5) based on (17-18).

The mechanical dynamics of the WRBDFIM are governed by the mechanical equation of rotation as in (19),

$$J_{tot}\frac{d\omega_{rm}}{dt} = T_{em} - T_L \tag{19}$$

where J_{tot} is the total inertia of the system, T_L is the load torque of the machine, and T_{em} is the sum of the electromagnetic torque produced by the MMWS and the CMWS, which is expressed in (20) based on the torque of a DFIM derived in [17].

$$\begin{aligned} T_{em} = {} & \frac{3}{2}\frac{P_1}{2}(\lambda_{ds1}i_{qs1} - \lambda_{qs1}i_{ds1}) \\ & + \frac{3}{2}\frac{P_2}{2}(\lambda_{ds2}i_{qs2} - \lambda_{qs2}i_{ds2}) \end{aligned} \tag{20}$$

For the purpose of machine simulation, (19) is also rearranged to a state equation in terms of the rotor mechanical speed state, as in (21).

$$\dot{\omega}_{rm} = (1/J_{tot})(T_{em} - T_L) \tag{21}$$

In summary, (12-15) and (21) together form the dynamics of the WRBDFIM. The whole 9^{th} order system of the WRBDFIM can be simulated by numerical methods.

V. Power Flow of The WRBDFIM

The power-flow in the WRBDFIM must be balanced based on the conservation of energy. The active power and reactive power of the stator MMWS and the stator CMWS are

$$P_{s1/2} = (3/2)(v_{ds1/2}i_{ds1/2} + v_{qs1/2}i_{qs1/2}) \tag{22}$$

$$Q_{s1/2} = (3/2)(v_{qs1/2}i_{ds1/2} - i_{qs1/2}v_{ds1/2}) \tag{23}$$

The active power flow in the WRBDFIM must be balanced; in other words, the input power must be equal to the output power of the WRBDFIM, which is shown in (24), (the core loss is neglected)

$$P_{s1} + P_{s2} = P_{em} + P_{cu1} + P_{cu2} \tag{24}$$

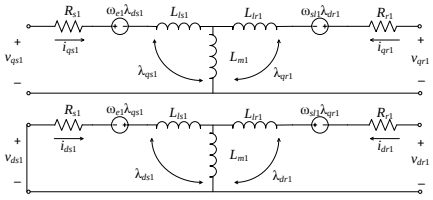

Fig. 7. The modified two-phase equivalent circuit of the MMWS according to the grid-flux orientation.

where

$$\begin{aligned} P_{cu1/2} = {} & (3/2)(i_{qs1/2}^2 r_{s1/2} + i_{ds1/2}^2 r_{s1/2} \\ & + i_{qr1/2}^2 r_{r1/2} + i_{dr1/2}^2 r_{r1/2}) \end{aligned} \tag{25}$$

$$P_{em} = T_{em}\omega_{rm} \tag{26}$$

where P_{em} is the electromagnetic power that is positive in the motoring direction and negative in the braking direction, P_{cu} is the copper loss, and T_{em} has been identified in (20).

VI. Direct Power Vector Control

Direct Power Vector Control (DPVC) is commonly used in conventional DFIMs to regulate the generated power and the power factor at the stator terminals connected directly to the grid. Most DPVC schemes use the stator flux orientation or the grid flux orientation. The stator flux orientation aligns the synchronous frame with the stator flux, whereas the grid flux orientation aligns the synchronous frame with the grid-voltage vector. It is evident that the stator flux frame is affected as the stator power varies. [14] The variation of the stator flux frame disturbs the decoupled property between the *dq*-control loops. [14] Therefore, The grid flux orientation is used in the proposed DPVC scheme for the WRBDFIM since the grid flux frame is always fixed to the grid voltage vector. [14]

The WRBDFIM is a combination of two DFIMs. In the two-phase domain, each winding set has its individual stator frame, rotor frame and synchronous frame. Since the *q*-phase stator MMWS is designed to be perfectly aligned with the *q*-phase stator CMWS, the two machine winding sets share the same stator frame, resulting in the five reference frames depicted in Fig. 6. Since the *q*-axis of the grid-flux synchronous frame aligns with the grid voltage vector with the same rotating speed, the *d*-component of the grid voltage is always zero. Consequently, the equivalent circuit of the MMWS must be altered according to the grid flux orientation. The modified two-phase equivalent circuit of the MMWS is shown in Fig. 7. The stator voltage of the CMWS can be calculated based on the grid power commands using the two-phase equivalent circuit of the WRBDFIM.

A. The desired stator current of the MMWS

In the grid-flux reference frame, the *dq* stator currents of the MMWS are directly proportional to the stator power. Since the v_{ds1} is zero, the relationship between the stator current of the

MMWS and the main machine stator power are reduced to the following by using (22-23)

$$P_{s1} = (3/2)(v_{qs1}^{e1} i_{qs1}^{e1}) \tag{27}$$

$$Q_{s1} = (3/2)(v_{qs1}^{e1} i_{ds1}^{e1}) \tag{28}$$

Assuming the desired grid active power and reactive power are P_{s1}^{*} and Q_{s1}^{*}, the required stator current can be calculated below by rearranging (27) and (28)

$$i_{qs1}^{e1*} = (2P_{s1}^{*})/(3v_{qs1}^{e1}) \tag{29}$$

$$i_{ds1}^{e1*} = (2Q_{s1}^{*})/(3v_{qs1}^{e1}) \tag{30}$$

B. The desired stator flux of the MMWS

The required stator flux to supply the desired grid power can be calculated based on the desired stator current. The stator voltage equations can be drawn based on Fig. 7, i.e.

$$v_{qs1}^{e1} = i_{qs1}^{e1} r_{s1} + \omega_{e1} \lambda_{ds1}^{e1} + \frac{d\lambda_{qs1}^{e1}}{dt} \tag{31}$$

$$0 = i_{ds1}^{e1} r_{s1} - \omega_{e1} \lambda_{qs1}^{e1} + \frac{d\lambda_{ds1}^{e1}}{dt} \tag{32}$$

By rearranging (31) and (32), the required stator flux of the MMWS can be calculated as

$$\lambda_{qs1}^{e1*} = \int v_{qs1}^{e1} - i_{qs1}^{e1*} r_{s1} - \omega_{e1} \lambda_{ds1}^{e1*} \tag{33}$$

$$\lambda_{ds1}^{e1*} = \int -i_{ds1}^{e1*} r_{s1} + \omega_{e1} \lambda_{qs1}^{e1*} \tag{34}$$

C. The desired rotor current of the MMWS

By the definition of the stator flux, the rotor current is related to the stator flux and stator current as shown below

$$\lambda_{qs1}^{e1} = L_{s1} i_{qs1}^{e1} + L_{m1} i_{qr1}^{e1} \tag{35}$$

$$\lambda_{ds1}^{e1} = L_{s1} i_{ds1}^{e1} + L_{m1} i_{dr1}^{e1} \tag{36}$$

If the desired stator current and the stator flux have been computed using (29), (30), (33), and (34), the desired rotor current can be identified by rearranging (35) and (36), as

$$i_{qr1}^{e1*} = (\lambda_{qs1}^{e1*} - L_{s1} i_{qs1}^{e1*})/L_{m1} \tag{37}$$

$$i_{dr1}^{e1*} = (\lambda_{ds1}^{e1*} - L_{s1} i_{ds1}^{e1*})/L_{m1} \tag{38}$$

D. The desired rotor flux of the MMWS

The desired rotor flux can be obtained based on its definition, since the desired stator current and rotor current have been identified. The desired *dq* rotor fluxes are

$$\lambda_{qr1}^{e1*} = L_{r1} i_{qr1}^{e1*} + L_{m1} i_{qs1}^{e1*} \tag{39}$$

$$\lambda_{dr1}^{e1*} = L_{r1} i_{dr1}^{e1*} + L_{m1} i_{ds1}^{e1*} \tag{40}$$

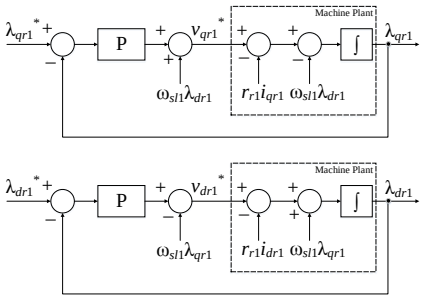

Fig. 8. Inner loop flux regulator of the MMWS.

E. The desired rotor voltage of the MMWS

Normally, calculating the desired rotor voltage using the rotor current and rotor flux involves the application of the differentiators, as in

$$v_{qr1}^{e1*} = \frac{d\lambda_{qr1}^{e1*}}{dt} + \omega_{sl1} \lambda_{dr1}^{e1*} + i_{qr1}^{e1*} r_{r1} \tag{41}$$

$$v_{dr1}^{e1*} = \frac{d\lambda_{dr1}^{e1*}}{dt} - \omega_{sl1} \lambda_{qr1}^{e1*} + i_{dr1}^{e1*} r_{r1} \tag{42}$$

In order to improve the dynamic response of the WRBDFIM, a flux regulator [14] is proposed, forming the inner feedback loop of the main *dq* control loop. The flux regulator is shown in Fig. 8. The main drawback of the flux regulator is the requirement that the instantaneous rotor flux be used as the feedback signal, which necessitates additional designs for the rotor-flux observer of the MMWS. The reason why only the proportional (P) control element is sufficient in the inner loop is because the integrator physically appearing in the machine plant can serve the purpose of eliminating the steady state error. [14] The control effort of the flux regulator is the rotor voltage of the MMWS.

F. The desired rotor voltage and current of the CMWS

The desired rotor voltage and current of the MMWS can be transferred to the CMWS. The rotor voltage and current of the CMWS can be obtained by computing a vector rotation as shown in Fig. 4, using (4) and (5). Thus, the desired rotor voltage and current are

$$v_{qr2}^{e2*} = v_{qr1}^{e1*} \tag{43}$$

$$v_{dr2}^{e2*} = -v_{dr1}^{e1*} \tag{44}$$

$$i_{qr2}^{e2*} = -i_{qr1}^{e1*} \tag{45}$$

$$i_{dr2}^{e2*} = i_{dr1}^{e1*} \tag{46}$$

The superscripts in (43-46) highlight the difference in frame of reference when making the transfer from the MMWS to the CMWS.

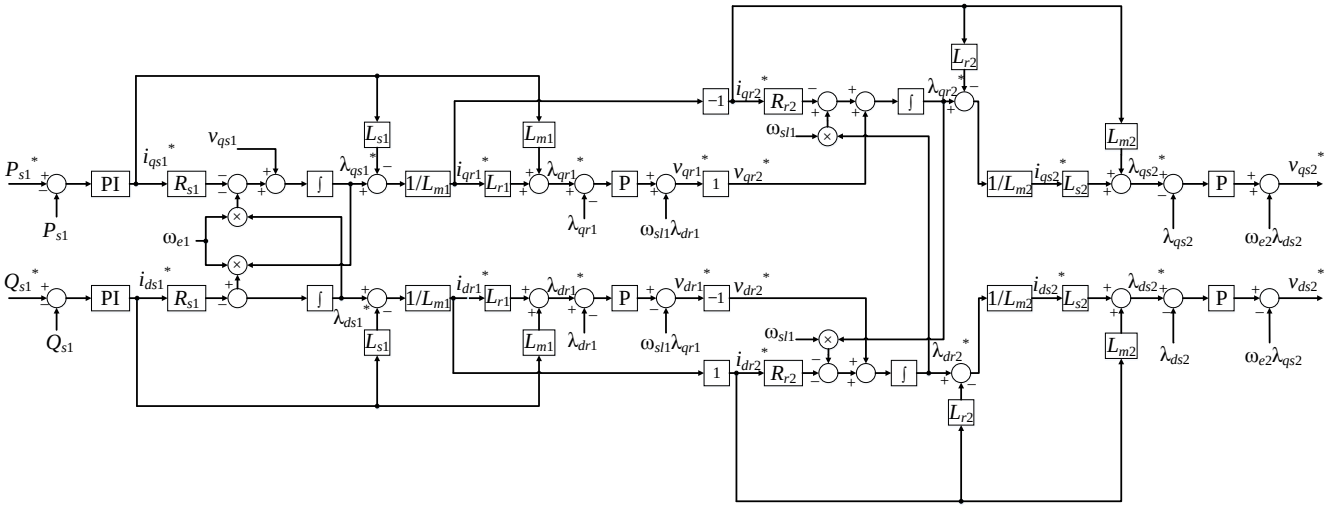

Fig. 9. The proposed DPVC scheme for the WRBDFIM.

G. The desired rotor flux of the CMWS

Using the same methodology as shown in (33-34), the desired rotor flux can be calculated based on the desired rotor voltage and current of the CMWS, as shown in (43-46). By following the equivalent circuits shown in Fig. 5, the desired *dq* rotor fluxes of the CMWS are

$$\lambda_{qr2}^{e2*} = \int v_{qr2}^{e2*} - i_{qr2}^{e2*} r_{r2} + \omega_{sl1} \lambda_{dr2}^{e2*} \tag{47}$$

$$\lambda_{dr2}^{e2*} = \int v_{dr2}^{e2*} - i_{dr2}^{e2*} r_{r2} - \omega_{sl1} \lambda_{qr2}^{e2*} \tag{48}$$

It should be noted that the speed of the synchronous frame of the CMWS must comply with the criterion given in (2). Therefore, the speed voltage source on the rotor side of Fig. 5 is evaluated to be equal to $-\omega_{sl1}$, which is directly used in (47) and (48).

H. The desired stator current and stator flux of the CMWS

In like manner, the desired stator current and stator flux of the CMWS are calculated by following the same methodology developed in (37-40). They are expressed as follows

$$i_{qs2}^{e2*} = (\lambda_{qr2}^{e2*} - L_{r2} i_{qr2}^{e2*})/L_{m2} \tag{49}$$

$$i_{ds2}^{e2*} = (\lambda_{dr2}^{e2*} - L_{r2} i_{dr2}^{e2*})/L_{m2} \tag{50}$$

$$\lambda_{qs2}^{e2*} = L_{s2} i_{qs2}^{e2*} + L_{m2} i_{qr2}^{e2*} \tag{51}$$

$$\lambda_{ds2}^{e2*} = L_{s2} i_{ds2}^{e2*} + L_{m2} i_{dr2}^{e2*} \tag{52}$$

I. The desired stator voltage of the CMWS

The calculation of the desired stator voltage of the CMWS also involves the application of the differentiators. The voltage equations on the stator side of the CMWS are

$$v_{qs2}^{e2*} = i_{qs2}^{e2*} r_{s2} + \omega_{e2} \lambda_{ds2}^{e2*} + \frac{d\lambda_{qs2}^{e2*}}{dt} \tag{53}$$

$$v_{ds2}^{e2*} = i_{ds2}^{e2*} r_{s2} - \omega_{e2} \lambda_{qs2}^{e2*} + \frac{d\lambda_{ds2}^{e2*}}{dt} \tag{54}$$

Again, another set of flux regulators are used here for each *dq* control loop in order to improve the dynamic response. The flux regulators are exactly the same as those of the MMWS, which are shown in Fig. 8. The instantaneous stator flux signal of the CMWS is also required, which must be obtained by observers. The control effort of the flux-controller is the voltage that drives the stator terminal of the CMWS.

J. Outer power feedback loop

The algorithm discussed so far is mainly the feed-forward portion of the DPVC. A set of proportional and integral (PI) controllers must be added as the outer feedback loops of the DPVC scheme to improve the stability and tracking capability of the WRBDFIM. The instantaneous values of the P_{s1} and Q_{s1} are used as the feedback signals, which can be easily measured on the stator winding of the MMWS. Since the PI controller is added as the outer feedback loop for each *dq* control loop, the proportionalities derived in (29) and (30) are already embedded in the PI control algorithm. Thus, the control effort of the PI controller is the desired stator current. The completed DPVC control scheme is shown in Fig. 9, which represents the feed-forward and outer feedback control algorithms pictorially using block diagrams.

VII. Simulation Results

The proposed 9^{th}-order dynamic model and the DPVC scheme of the WRBDFIM are simulated in Simulink using the two machines detailed in Table I. The voltage of the grid-connected stator of the MMWS is set to its rated terminal voltage of 220V (line-line RMS at 60 Hz). The stator terminals of the CMWS are directly connected to the output of the DPVC. The numerical method is set to the 'Stiff-Rosenbrock' method in the ODE solver, with the relative tolerance set to '1e-6'.

TABLE I
WINDING SETS SPECIFICATIONS

	MMWS Parameters	CMWS Parameters
Pole Pairs P	2	1
Rated Frequency f_e (Hz)	60	60
Rated Power P_R (kW)	3.73	3
Rated Voltage (LL) V_s (VRMS)	220	220
Connection	Star	Star
Stator Resistance R_s (Ω)	0.531	0.403
Stator Leakage Inductance L_{ls} (H)	0.00252	0.0039
Magnetizing Inductance L_m (H)	0.0847	0.128
Rotor Resistance R_r (Ω)	0.408	0.484
Rotor Leakage Inductance L_{lr} (H)	0.00252	0.0039
Fictitious Resistance R_f (Ω)	100000	
Total Inertia J_{tot} (kgm^2)	0.2	

TABLE II
FINE-TUNED CONTROLLER GAINS

	q-loop Values	d-loop Values
Outer-loop P Gain K_{Po}	0.8	0.05
Outer-loop I Gain K_{Io}	17	36
Inner-loop MMWS P Gain K_{Pi1}	0.15	0.15
Inner-loop CMWS P Gain K_{Pi2}	0.1	0.1

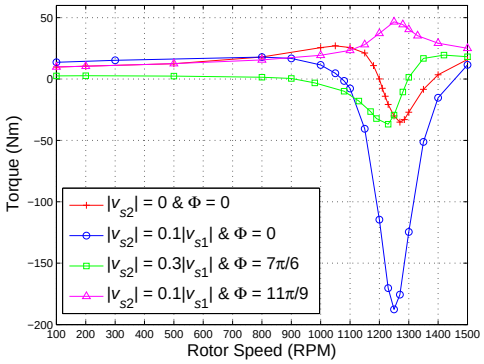

Fig. 10. Torque-Speed curves of the WRBDFIM with different v_{s2}.

A. Steady-state performance

The steady-state performance of the WRBDFIM can be obtained by disabling the mechanical dynamics of the machine model, leaving only the remaining 8^{th}-order electrical dynamics active. The rotor speed can be set to any constant values, as can the voltage source that drives the stator terminals of the CMWS. The grid-connected stator voltage of the MMWS is fixed to its rated voltage. The electromagnetic torque of the WRBDFIM is computed by using (20), where the current and flux states are simulated by the constant speed dynamic model of the WRBDFIM.

Fig. 10 shows the steady-state torque speed curve obtained using the constant speed simulation model of the WRBDFIM. The torque speed curve is essentially a summation of two individual torque-speed curves having different pole numbers. From Fig. 10, it is evident that the torque-speed curves vary as the magnitude ($|v_2|$) and the phase-shift (ϕ) change, making the WRBDFIM suitable for wind turbine applications. When 'v_{s2} = 0', the WRBDFIM acts a cascaded induction machine. The synchronous speed, i.e. 1200 RPM shown in Fig. 10, exactly matches the synchronous speed predicted using (3).

B. Dynamic response to a step change in stator power

To investigate for the transient response to a step change in stator power, the rotor speed of the WRBDFIM model is no longer set to a constant. Both the electrical and mechanical dynamics are now active in the machine model, resulting in a 9^{th}-order system. The excitation at the stator terminal of the MMWS remains at the rated voltage. The output of the controllers directly drives the stator terminals of the CMWS. The proposed DPVC scheme for the WRBDFIM utilizes the instantaneous values of P_{s1}, Q_{s1}, λ_{qr1}, λ_{dr1}, λ_{qs2}, and λ_{ds2} as the feedback signals. In practice, P_{s1} and Q_{s1} can be measured by power meters at the stator terminal of the MMWS. λ_{qr1}, λ_{dr1}, λ_{qs2}, and λ_{ds2} must be observed using the stator current and voltage available at the stator terminals of the MMWS and CMWS. For simulation purposes, the P_{s1} and Q_{s1} can be calculated using the flux states of the machine model based on (22-23), whereas λ_{qr1}, λ_{dr1}, λ_{qs2}, and λ_{ds2} are the flux states of the machine model listed in (12-15).

The gains of the controllers are fine-tuned, and summarized in Table II. Before the stator power references of the MMWS are suddenly changed, the machine is running at 1120 RPM with no load. At t = 0.5 s, the active power reference and reactive power reference suddenly change to -3730 W and 1807 Var respectively, resulting in a power factor equal to 0.9, lagging. The load torque is set to -32.4 Nm at t = 0.5 s, which is the same as the T_{em} produced by the WRBDFIM in its steady-state.

The transient active power and reactive power response to the sudden change in the grid power references are shown in Fig. 11 and Fig. 12, respectively. The power responses of the WRBDFIM show 0% overshoot and 0% steady-state error. The active power and reactive power take 0.3 s and 0.35 s to reach steady-state, respectively. The corresponding torque and speed of the WRBDFIM are also shown in Fig. 13 and Fig. 14, respectively. Since the load torque has been set to equal to the electromagnetic torque, the rotor speed is stable in the steady-state, as indicated in Fig. 14.

VIII. CONCLUSION

In this paper, an alternative type of BDFIM is proposed, aiming to eliminate the circulating stator current due to magnetic unbalance in the single stator winding sets of conventional BDFIMs and effectively suppress the unwanted harmonics created by nest-loop rotor. The proposed WRBDFIM is easier to manufacture comparing to the conventional BDFIMs. A vector rotation is derived for the junction circuit between the MMWS and the CMWS. In order to construct a

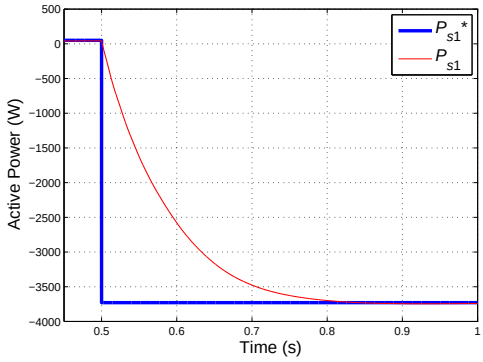

Fig. 11. Active power response to a step change in grid power.

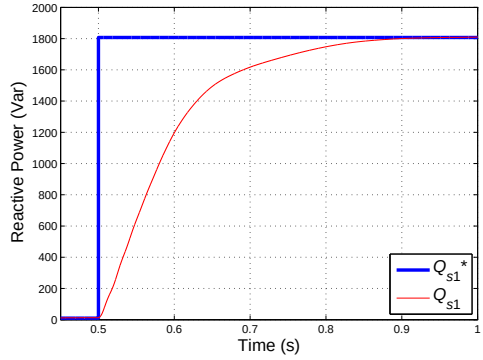

Fig. 12. Reactive Power response to a step change in grid power.

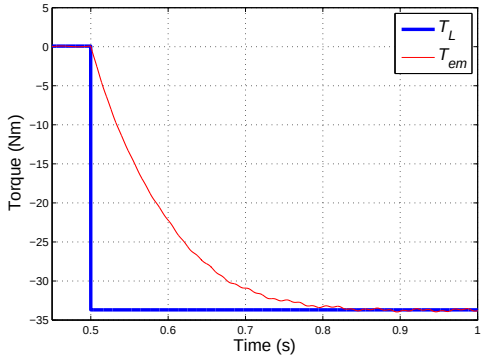

Fig. 13. Electromagnetic torque response to a step change in grid power.

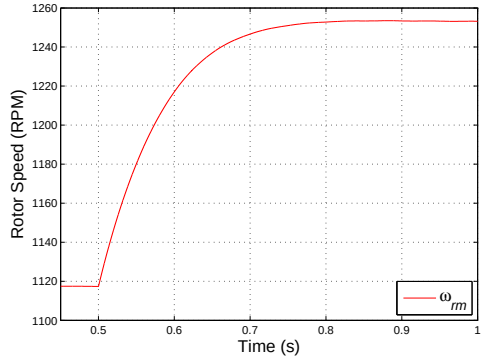

Fig. 14. Rotor speed response to a step change in grid power.

machine model for the DPVC, the electrical and mechanical dynamics of the WRBDFIM are identified, forming a 9^{th}-order dynamic system. In order to maintain the grid power level, and also to improve the dynamic response and the tracking capability of the WRBDFIM, the new DPVC scheme without rotor position sensors is proposed. Simulation results verify the dynamic model of the WRBDFIM and the proposed DPVC. The simulation results show a fast and accurate response to a step change in the stator power references of the MMWS. The effectiveness of the DPVC and the elimination of brushes and slip rings prove that the WRBDFIM has considerable potential in wind turbine applications.

REFERENCES

[1] G. A. Abrad, J. Lopez, M. Rodriguez, L. Marroyo, G. Iwanski, *Doubly Fed Induction Machine: Modeling and Control for Wind Energy Generation*, Wiley, NJ: IEEE Press, 2011, pp. 25.

[2] T. A. Lipo, "A supersynchronous doubly fed induction generator option for wind turbine applications," in *Power Electronics and Machines in Wind Applications Conf.*, Lincoln, NE, 2009, pp. 1-5.

[3] L. Hunt, "A new type of induction motor," *Proc. IET*, vol. 39, no. 186, pp. 648-667, March, 1907.

[4] A. Boardway, L. Burbridge, "Self-cascaded machine: a low-speed motor or high-frequency brushless alternator," *Proc. IEE*, vol. 117, no. 7, pp.1277-1290, July, 1970.

[5] A. Kusko, C. Somuah, "Speed Control of a Single-Frame Cascade Induction Motor with Slip-Power Pump Back," *IEEE Trans. Ind. Appl.*, vol. IA-14, no. 2, pp. 97-105, Apr., 1978.

[6] W. R. Brassfield, R. Spee, T. G. Habetler, "Direct Torque Control for Brushless Doubly-Fed Machines," *IEEE Trans. Ind. Appl.*, vol. 32, no. 5, pp. 1098-1104, Oct. 1996.

[7] F. Runcos, R. Carlson, A. M. Oliveira, P. Kuo-Peng, N. Sadoski, "Performance analysis of a Brushless Double Fed Cage Induction Generator," in *Nordic Wind Power Conference*, Goteborg Sweden, 2004, pp. 1-8.

[8] F. Barati, R. McMahon, S. Shao, E. Abdi, H. Oraee, "Generalized Vector Control for Brushless Doubly Fed Machines With Nested-Loop Rotor," *IEEE Trans. Ind. Electron.*, vol. 60, no. 6, pp. 2477-2485, Jun. 2013.

[9] P. Rochelle, R. Spee, A. K. Wallace, "The effect of stator winding configuration on the performance of brushless doubly-fed machines in adjustable speed drives," in *Industry Applications Society Annual Meeting*, Seattle, WA, 1990, pp. 331-337.

[10] S. Williamson, A. C. Ferreira, A. K. Wallace, "Generalised theory of the brushless doubly-fed machine. Part 1: Analysis," *Proc. IEE. Elect. Power Appl.*, vol. 144, no. 2, pp. 111-122, Mar. 1997.

[11] A. Broadway, "Cageless induction machines," *Pro. Inst. Elect. Eng.*, vol. 118, pp. 1593-1600, Nov. 1971.

[12] L. Xu, F. Liang, T. A. Lipo, "Transient model of a doubly excited reluctance motor," *IEEE Trans. Energy Conv.*, vol. 6, pp. 126-133, Mar. 1991.

[13] R. E. Betz, M. G. Jovanovic, "The brushless doubly fed relectance machine and the synchronous reluctance machine - comarison," *IEEE Trans. Ind. Appl.*, vol. 36, pp. 1103-110, Jul/Aug. 2000.

[14] N. Amiri, S.M. Madani, T.A. Lipo, H.A. Zarchi, "An Improved Direct Decoupled Power Control of Doubly Fed Induction Machine Without Rotor Position Sensor and With Robustness to Parameter Variation," *IEEE Trans. Energy Conv.*, vol. 27, no. 4, pp. 873-884, Dec. 2012.

[15] D. Zhou, R. Spee, G. C. Alexander, "Experimental evaluation of a rotor flux oriented control alogrithm for brushless doubly-fed machines," *IEEE Trans. Power Electron.*, vol. 12, no. 1, pp. 72-77, Jan. 1997.

[16] B. Hopfensperger, D. J. Atkinson, R. A. Lakin, Stator flux oriented control of a cascaded doubly-fed induction machine, *Proc. Inst. Elect. Eng.Elect. Power Appl.*, vol. 146, no. 6, pp. 597-605, Nov. 2006.

[17] D. W. Novotny, T. A. Lipo, *Vector Control and Dynamics of AC Drives*, Oxford Science Publication, NY: Oxford University Press, 1996, pp. 75.